Intelligent Systems with Applications 14 (2022) 200067

Contents lists available at ScienceDirect

Intelligent Systems with Applications

journal homepage: www.elsevier.com/locate/iswa

Forecasting design values of tidal/ocean power generator in the strait with unidirectional flow by deep learning

Ryo Fujiwara [a,*], Ryoma Fukuhara [b], Tsubasa Ebiko [c], Makoto Miyatake [d]

[a] Dept. of Production Systems Engineering, National Institute of Technology, Hakodate College, 14-1 Tokura-cho, Hakodate, Hokkaido, Japan
[b] OEM group, Production Team, MEDEC Co., Ltd., 3-133 Suzuranoka-cho, Hakodate, Hokkaido, Japan
[c] Techno-Training Center, National Institute of Technology, Hakodate College, 14-1 Tokura-cho, Hakodate, Hokkaido, Japan
[d] Dept. of Civil Engineering, National Institute of Technology, Hakodate College, 14-1 Tokura-cho, Hakodate, Hokkaido, Japan

ARTICLE INFO

Article history:
Received 3 October 2021
Revised 24 December 2021
Accepted 9 February 2022
Available online 11 February 2022

Keywords:
Tidal power generator
Ocean power generator
Forecasting design values
Deep learning

ABSTRACT

Renewable energy is an essential factor in guaranteeing the sustainability of society. In Japan, there have been developments to harness energy from the ocean. The Tsugaru strait, in the northern region of Japan, is an area that has attracted attention for this purpose. We propose a tidal/ocean power generator utilizing a Flaring Flanged Diffuser (FFD) to harness the power. However, for the power generators utilizing FFD to generate power at the optimal condition, design values based on the stream regimes need to be determined. In this paper, the objective is to forecast the design values of tidal/ocean power generators utilizing FFD. We are especially interested in the dimensions of the diffuser shape that relate to effective factors for increasing flow velocity. Fluid field data around FFD is obtained by experimentation. The fluid field data is measured by particle image velocimetry (PIV). The trained deep neural network can forecast design values from a given fluid field. Moreover, we can recognize correlations between the changes in design values and the increase of fluid velocity.

© 2022 The Author(s). Published by Elsevier Ltd.
This is an open access article under the CC BY-NC-ND license
(http://creativecommons.org/licenses/by-nc-nd/4.0/)

1. Introduction

Renewable energy is an essential factor in guaranteeing the sustainability of society. At present, almost all of the energy in the world relies on fossil fuels. Renewable energy is expected as a replacement for non-renewable energy sources.

To effectively harness the energy in any condition, researchers need to predict the trend of natural phenomena. Mathematical models are used to predict a trend of flow (e.g., tidal flow, wind). Liu, Li, Billinton, Wang and Yu (2015) use Wakeby distribution for the modeling of tidal current speed. Jónsdóttir and Milano (2020) constructed stochastic models to predict wind power fluctuations and tidal flow power in the all-island Irish transmission system. To efficiently obtain energy from the source, there have been also attempts to control the power plant by mathematical models. Marei, Mokhtar and El-Sattar (2015) propose the MPPT (maximum power point tracking) strategy of AWS (Archimedes wave swinging)-based wave energy conversion system . The unscented Kalman filter algorithm is used to estimate the float velocity. Suchithra, Ezhilsabareesh and Samad (2019) propose the BEPT (best efficiency point tracking) method of wave energy converter by higher-order sliding mode controller. Lust, Bailin and Flack (2021) performed the model experiment of the H-Darrieus cross-flow hydrokinetic turbine. Han, Jung and Hwang (2021) clarified the optimal layout of a tidal current turbine farm in a shallow channel to maximize power production by numerical simulation. High-resolution rapid refresh model and computational fluid dynamics are used to study dynamic line ratings (Abboud et al., 2019). Bayesian network is used to forecast load (Bessani, Massignan, Santos, London & Maciel, 2020). These studies are conducted by using mathematical models without the use of machine learning.

On the other hand, machine learning is focused as one of the methods to manage renewable energy. There have been studies of machine learning for forecasting ocean energy, like wave energy and tidal energy. Bento, Pombo, Mendes, Calado and Mariano (2021) optimized deep learning neural networks to forecast the wave energy flux and other wave parameters. Moth-frame optimization is used to modulate configurations of networks and input data. Aly forecasts tidal current constitution by a hybrid

* Corresponding author.
E-mail addresses: r_fujiwara@hakodate-ct.ac.jp (R. Fujiwara), t.ebiko@hakodate-ct.ac.jp (T. Ebiko), miyatake@hakodate-ct.ac.jp (M. Miyatake).

https://doi.org/10.1016/j.iswa.2022.200067
2667-3053/© 2022 The Author(s). Published by Elsevier Ltd. This is an open access article under the CC BY-NC-ND license
(http://creativecommons.org/licenses/by-nc-nd/4.0/)

model of wavelet neural network, artificial neural network (ANN), Fourier Series based on least squares, and Recurrent Kalman Filter (Aly, 2020b). Machine learning is also used to control ocean power plants. Amundarain, Alberdi, Garrido, Garrido and de la Sen (2012) controlled a wave power plant by ANN and improved performance during voltage dips in the grid. M'zoughi, Garrido, Garrido, La Sen and De La (2020) constructed an ANN-based airflow control system of oscillating water column (OWC) to prevent stalling phenomena. This ANN forecasts the velocity of airflow from the amplitude and period of the wave. M'zoughi, Garrido, Garrido and De La Sen (2020) constructed a rotational speed control system of the turbine in OWC by ANN-based MPPT. This ANN forecasts the rotational speed of the turbine from the amplitude and period of the wave. Ghefiri, Bouallègue, Garrido, Garrido and Haggège (2018) Forecast the proper rotational speed and the blade pitch angle of tidal stream generator from the flow velocity by multi-layer ANN. In addition, machine learning is used to forecast wind velocity and energy (Bastos, Oliveira & Milidiú, 2021; Gan, Li, Zhou & Tang, 2021; Liu, Zhou & Qian, 2021; Toubeau et al., 2021). These forecasts can be used for the control of wind power plants. Machine learning is also used in PV (Photovoltaic) systems as a battery smoothing controller using total sky images (Ryu, Ishii & Hayashi, 2021). The load, where to use energy, is also forecasted by machine learning (Aly, 2020a; Atef & Eltawil, 2020; Chen, Wang, Wang & Li, 2019; Khwaja, Anpalagan, Naeem & Venkatesh, 2020; Memarzadeh & Keynia, 2021; Sideratos, Ikonomopoulos & Hatziargyriou, 2020; Wen, Xie, Fan & Feng, 2020b, 2020a; Zheng, Wang, Liu & Liu, 2019; Zhu, Geng & Wang, 2021). There has also been a study of load disaggregation by machine learning (Xia, Wang, Zhang & Xu, 2019). Machine learning is used in not only engineering but economics. Riddervold, Riemer-Sørensen, Szederjesi and Korpås (2020) propose methods to predict the bidding strategy in reservoir hydro.

In this study, we focus on ocean energy, especially the energy from ocean/tidal flow. According to the review article on ocean power technology by Wilberforce et al. (2019), the potential estimate for tidal energy was given as 3TW. Ocean energy plants have merits: the equipment space does not require land use, which can be expensive or scarce, and the energy density is higher than air. The social acceptance of ocean energy is considered. The case study of an OWC shoreline plant of Mutriku provides an analysis of the social acceptance of ocean energy plants (Heras-Saizarbitoria, Zamanillo & Laskurain, 2013). In Japan, there are developments to harness energy from the ocean. In the southern region of Japan, there is a 100 kW class prototype subsea floating type ocean current power generation system "Kairyu." The demonstration test of Kairyu was conducted in the waters off the coast of Kuchinoshima, Toshima, Kagoshima Prefecture New Energy and Industrial Technology Development Organization (2021).

The Tsugaru strait, in the northern region of Japan, is an area that has attracted attention for the utilization of tidal/ocean energy. Unidirectional tidal and ocean flow with high energy density drifts between the main island and Hokkaido Island. Energy harvesting, equipping multiple tidal/ocean power generators in The Tsugaru strait, has shown to be effective. There have been many ways in which these methods can be improved. We propose a tidal/ocean power generator utilizing a Flaring Flanged Diffuser (FFD), as shown in Fig. 1, to harness the power effectively. The flaring shape and the flange increase the tidal/ocean flow velocity, and stable energy can be extracted.

However, for the power generators utilizing FFD to generate power in the optimal condition, design values based on the stream regime need to be determined. Although there have been some control methods of ocean power generators, a method to forecast design value has not yet been established. Our research group investigates the optimal designing of tidal/ocean power generator by

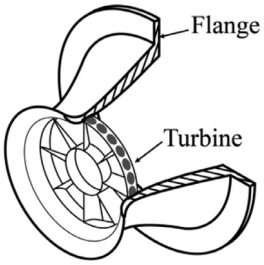

Fig. 1. Schematic illustration of tidal/ocean power generator with "Flaring Flanged Diffuser" (FFD).

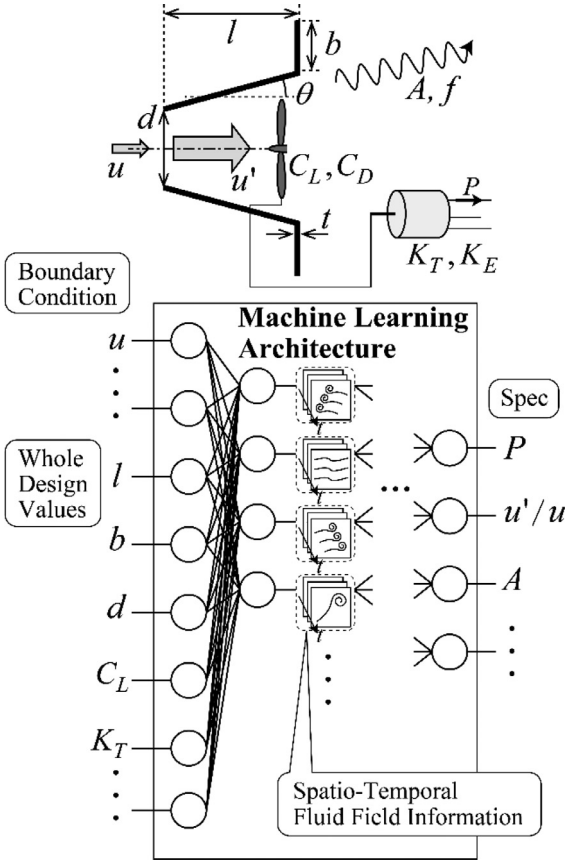

Fig. 2. The concept illustration of machine learning architecture to optimize designing of tidal/ocean power generator.

machine learning architecture. The concept of whole structure is shown in Fig. 2.

The architecture inputs boundary condition and whole design values, and outputs the spec of the tidal/ocean power generator. In the hidden layer, spatio-temporal fluid field information is considered. As a first step, the relation between fluid field and design value is needed.

In this paper, the objective is to forecast the design value of tidal/ocean power generators utilizing FFD. We are especially interested in the dimensions of the diffuser shape that relate to effective factors for increasing flow velocity. This is our new challenge and there are no comparisons. To achieve the objective, deep learning is used to describe the relationship between the velocity field and the design values. To obtain learning data, model experiments based on measurement in The Tsugaru strait are conducted. First, movies of fluid flow with particles are recorded by a high-speed camera in model experiments by a 2-dimensional slitted tank. For simplicity, we conducted a 2-dimensional experiment. Second, the

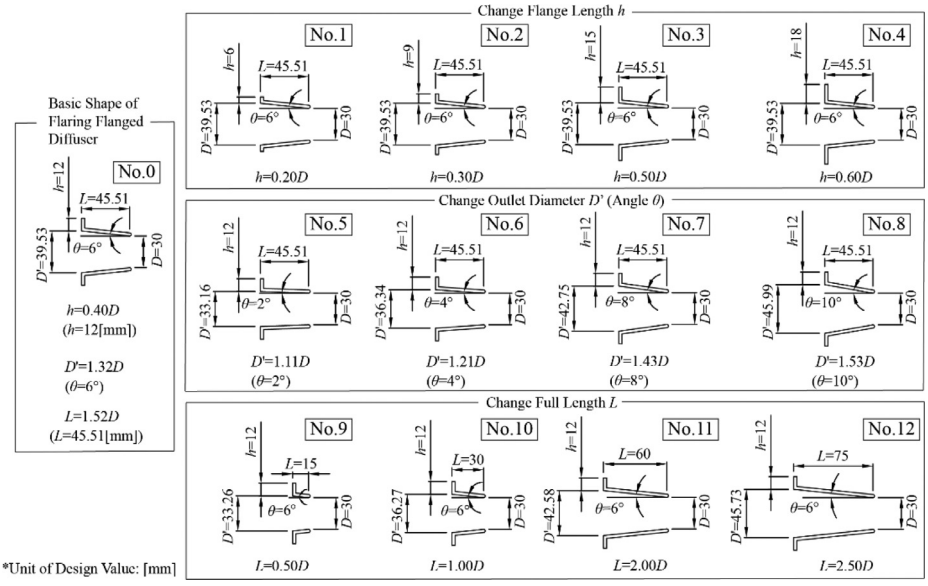

Fig. 3. Shapes of Flaring Flanged Diffuser (FFD) model. No. 0 is the basic shape of the diffuser. Flange length h, outlet diameter D' (that depends on opening angle), and full-length L are changed, respectively.

data of flow velocity field is obtained by the particle image velocimetry (PIV) method. Then, deep learning describes the relationship between input data and output data. The velocity field data is input data, and the design value data is output data. Finally, a trained deep neural network can forecast design values.

2. Materials and methods for measuring fluid field

Fluid field data around the Flaring Flanged Diffuser (FFD) is obtained in experiments. The fluid field data is measured by particle image velocimetry (PIV). In this section, the details of the experimental operations are explained.

2.1. Materials

First, the diffuser model is manufactured as follows. Fig. 3 shows the shapes of the FFD model.

Mehmood, Liang and Khan (2012) clarified that a flaring diffuser increases fluid velocity. The jet stream would be generated by the low internal pressure that is caused by the uplifting effect of the flaring shape. In addition, we confirmed that a stable jet stream is being generated by adding a flange on the outlet of the diffuser. Ring vortex is generated downstream. This ring vortex would extend the low-pressure region. Considering these acceleration effects of fluid velocity, FFD is employed in this study.

Two-dimensional FFD models are manufactured by changing Flange length h, outlet diameter D', and full-length L based on the basic shape of the diffuser, No. 0 as shown in Fig. 3. Note as an aside, outlet diameter D' depends on opening angle. These models are made from a clear acrylic resin. The width of the model is 40 mm, which is the same as the width of the tank used in experiments. Then, the model experiments are conducted in a steady flow circulation tank, as shown in Fig. 4. The circulation tank is made of acrylic resin and has a rectifier board with holes in its inlet and outlet. A magnet pump generates the steady flow of the tank with a maximum flow rate of 900 cm^3/s.

2.2. Methods

Fluid field data is measured by PIV as follows. First, mainstream velocity is modified by generating steady flow circulation without a diffuser. The velocity is modified based on the flow conditions of the Tsugaru Strait. In the Tsugaru strait, the energy density is minimized in summer duration. The fluid velocity is 87.7 cm/s at a depth of 10 m in this duration. The fluid velocity in the model is downscaled as 16.5 cm/s, $1/\sqrt{28}$ of original velocity, by Froude similarity. To conduct PIV, polystyrene particles with a diameter of 70 μm (Thermo Fisher, 4230A) are dispersed in the tank. A blue laser irradiates the particles with 1 W power to observe their motion. A high-speed camera with a frame rate of 200 fps (Direct, HAS-L1) is used to record the movies of the motion of the particles irradiated by a blue laser.

By analyzing the movies (continuous images) by PIV, the fluid field data is obtained. ImageJ, image processing software, is used in PIV analysis. PIV analysis confirmed that main stream velocity reaches target value (16.5 cm/s) with 750cm^3/s of pump's flow rate. And then, the FFD model is installed as shown in Fig. 4. The fluid field data is obtained by observing flow conditions around the model using PIV. Since the tank and the diffuser model are made from clear acrylic resin, the blue laser can pass through the regions of the diffuser model. It is confirmed that the effect of scattered light is negligible. The coordinate is set as Fig. 4. The origin O is at the bottom of the downstream, the positive direction of the x-axis points to the upstream, and the positive direction of the z-axis points upward in a vertical direction.

3. Making data of fluid field and forecasting design values

3.1. Making data of fluid field

Using the fluid field data obtained by the experiment, the relation between the FDD model's fluid field and design values is learned by a deep learning model. The learned deep neural network can forecast design value from the desired fluid field. The environment of machine learning is as follows. Python is used as a programming language. Integrated development environment Jupyter Notebook is used to write and execute the program.

The fluid field data is stored in NumPy arrays in the Python programming language. Before the execution of deep learning, it is needed to store the data in an array. The experimental data, coordinate value (x and z), and horizontal/vertical velocity speed (u and v) are recorded in a CSV file. The CSV interface library in Python is

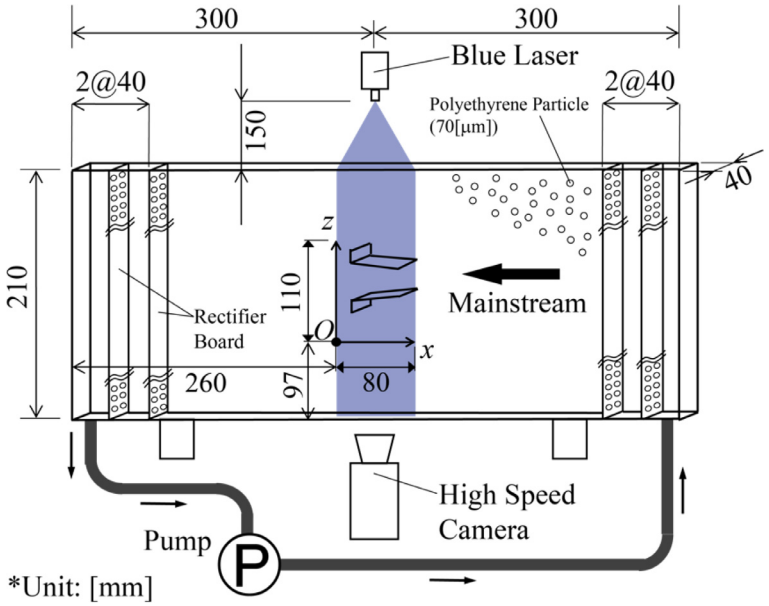

Fig. 4. Experimental setting with steady flow circulation tank.

Table 1
Quantities of meshes of position data.

No. of Diffuser Shape	x range	y range
0	35	47
1	36	47
2	36	47
3	35	47
4	35	47
5	35	47
6	35	47
7	35	47
8	35	47
9	35	48
10	35	47
11	35	47
12	48	47

used to store the data. The quantity of meshes of position data depends on the shape of the diffuser model as Table 1.

Thus, to store whole data, a 3-dimensional array with the shape of $2 \times 48 \times 48$ is adopted. The first element indicates the direction of velocity, u and v. The second and third elements respectively indicate the x and z position. In deep learning, only horizontal velocity u is used. The quantity of movie frames and shape variations are also considered. The shortest movie has 4900 frames. 13 kinds of diffuser models were made. Thus, the whole tensor shape is $2 \times 13 \times 4900 \times 48 \times 48$. The detail of the fluid field tensor shape is shown in Fig. 5.

In learning by the deep neural network, the fluid field data is inputted as a one-dimensional tensor. Fluid velocity series on the x-axis at $y = 0$ are stored in an array, and this operation is repeated by changing the value of y. This fluid field tensor is transformed by function f to input fully connected neural network as follows.

$$f : \mathrm{R}^{n_d \times n_v \times n_t \times n_x \times n_y} \rightarrow \mathrm{R}^{n_d n_v n_t \times n_x n_y} \tag{1}$$

where n_d denotes the number of diffuser shapes, n_v denotes the number of fluid flow directions, n_t denotes the number of time frame, n_x denotes the number of segments for x-axis, and n_y denotes the number of segments for y-axis, respectively. In deep learning, the number n_v is one since only horizontal velocity u is used. The number $n_d n_v n_t$ denotes the number of sample data. The

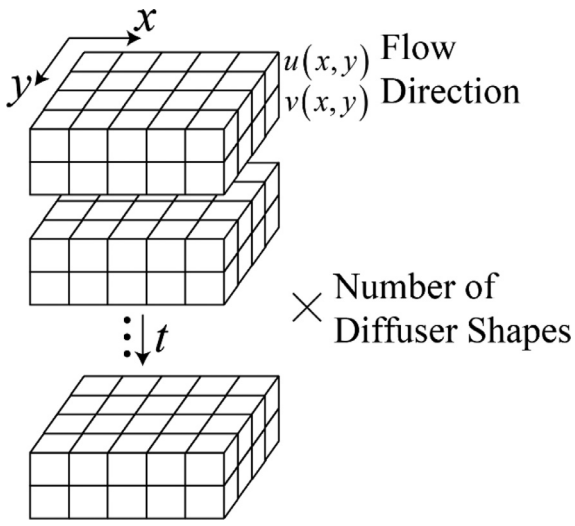

Fig. 5. The detail of the fluid field tensor shape. The tensor has 5 dimensions. In deep learning, only horizontal velocity u is used.

number $n_x n_y$ denotes the size of tensor that is inputted to a deep neural network.

Fig. 6 shows a screenshot of the movie and a color gradation of stored data. By comparing the movie and the stored data, it is confirmed that the data can describe the fluid field since the fluid velocity in the central region is higher than the velocity of the upper and bottom region. To conduct deep learning, it is better to normalize the data to be within the region of $[-1, 1]$ (Chollet, 2017). Thus, all velocity data is divided by the maximum flow speed in the data. Performing the above processing, 127,400 sets of fluid field data are obtained from the data by PIV analysis. Fig. 6(b) shows the color contour of experimental data. The color gradation shows the magnitude of the horizontal fluid velocity u. The red color indicates a faster one, and the blue color indicates a slower one. The white color indicates average velocity. Originally, there is no fluid velocity in the region covered by the diffuser. However, to input a deep learning network, this region has the average velocity as padding data. In the same way, the region outside of the data

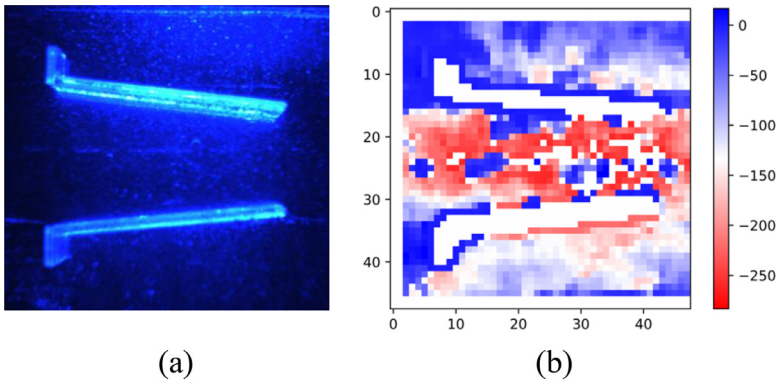

Fig. 6. (a)Screenshot of the movie and (b)color contour of fluid field in experiment.

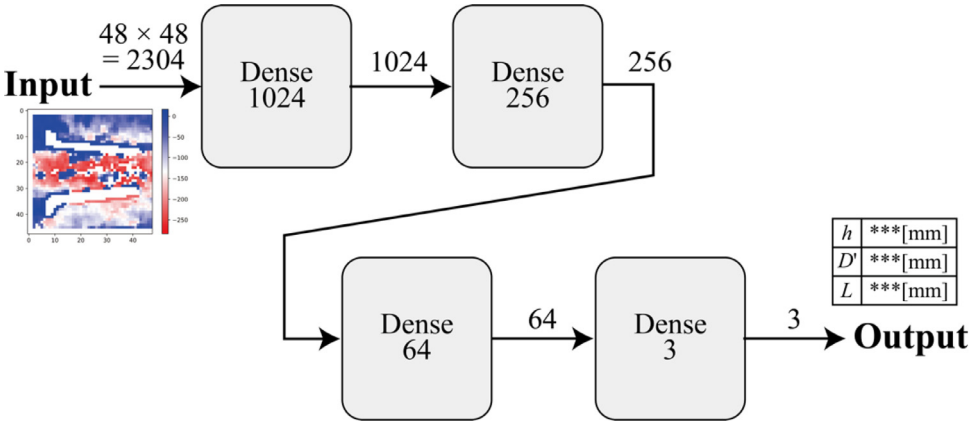

Fig. 7. Schematic diagram of the deep neural network to forecast design values. The size of the tensor is compressed from 2304 to 1024, 256, 64, and 3 by going through the dense layer.

range has the average velocity as padding data. As shown in Fig. 6(b), the fluid velocity in the central area is faster, and the velocity is slower on the downside and upper side. Thus, the increase of fluid velocity is observed.

3.2. Architecture of deep learning for forecasting design values

By using a deep neural network, the design value forecast is performed from fluid field data. The schematic diagram of the architecture of the deep neural network is shown in Fig. 7. Dense layers are adopted. The relation between the input and the output of the layer is as follows.

$$z_{n+1} = \sigma(W_n z_n + b_n), \tag{2}$$

where z_n *and* z_{n+1} denotes the input and output tensor respectively. W_n and b_n denote the weight and bias tensor respectively. Function s is sigmoid function as follows.

$$\sigma(s) = \frac{1}{1+e^{-s}}, \tag{3}$$

where s denotes a variable. In the calculation, this function is applied to each element in the variable tensor. To smoothly output the design value data and adequately compress the information, the quantity of nodes (the size of output tensor) smoothly decreases from the quantity of input data to that of output data. Binary cross-entropy $B(T,z_n)$ is used as the loss function. Function $B(T,z_n)$ is as follows.

$$B(T_i, z_{N,i}) = -[T_i \log(z_{N,i}) + (1-T_i)\log(1-z_{N,i})], \tag{4}$$

Where T_i is true value, and $z_{N,i}$ is predicted value on the output of final layer. i denotes element number of the output of final layer, and it also denotes flange length h, outlet diameter D', or full-length L. Adam (Kingma & Ba, 2014) is used to search minimal value of the loss function for adjusting weight tensor W_n and bias tensor b_n. This is a simple way of deep learning, however, this method could be applied to the design of tidal/ocean power generator.

By using the trained deep neural network, forecasting design values from a given fluid field is performed. In the strait with various fluid fields, a flexible design method is needed. The trained deep neural network would be a good guideline to search optimal design values to increase fluid velocity magnitude. To perform a search of optimal design values, evaluations of the deep neural network are conducted as follows. First, the errors in 13 kinds of diffusers are obtained by inputting given training data (fluid field). Second, forecasted design values are evaluated by inputting the unknown data of which fluid velocity is changed.

4. Results and discussions

A deep neural network is trained to fit the fluid field data and design value data. Accumulating epochs, the accuracy goes 100%, and the loss goes 0.478. The neural network needs 30 epochs of learning to obtain enough accuracy to forecast design values.

4.1. Evaluation of error for forecasting design values

Design values are forecasted by the learned deep neural network. In this section, the error between forecast value and experimental given value is discussed. For every thirteen kinds of diffuser design, ten fluid field data are randomly sampled. The design

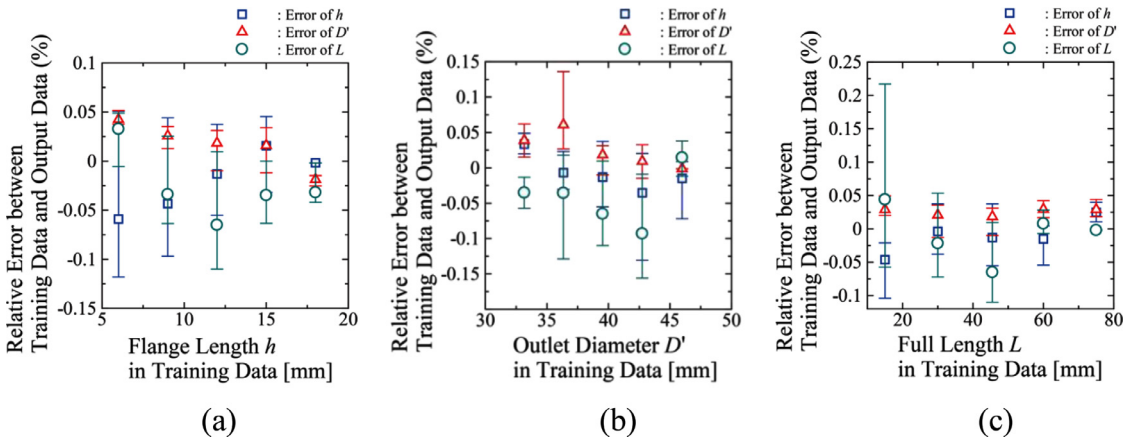

Fig. 8. Comparisons of forecast errors of flange length h, outlet diameter D', and full-length L. Horizontal axis shows design value h, D,' and L on (a), (b), and (c), respectively. The vertical axis shows forecast error by the deep neural network.

values are forecasted using these 130 data. Fig. 8 shows comparisons of the errors. The horizontal axis shows design values h, D', and L. Vertical axis shows forecast error by the deep neural network. A plot shows the average error of 10 forecast values. An error bar shows the maximum and minimum errors. The errors are within almost ±0.1%. Thus, it could be expected that design values are forecasted with high accuracy using unknown fluid field data such as interpolation of experimental data.

Figure 8(a) shows the comparison of forecast errors of h, D', and L by changing flange length h. Increasing flange length h, the error decreases to near 0%. This would be because of flow stability. Increasing flange length h, the flow outside of diffuser is difficult to disturb the flow inside of diffuser. Because of this effect, the flow inside of diffuser is stable. Thus, the recognition of fluid field data would be easier. Figure 8(b) shows the comparison of forecast errors of h, D', and L by changing outlet diameter D.' There is an outlier in the errors. This is because the fluid field data that is difficult to recognize would be sampled. Figure 8(c) shows the comparison of forecast errors of h, D', and L by changing full-length L. Increasing full-length L, the error decreases to near 0%. This would be because of flow stability. Increasing whole length L, the flow outside of diffuser is difficult to disturb the flow inside of diffuser. Because of this effect, the flow inside of diffuser is stable. Thus, the recognition of fluid field data would be easier.

4.2. Forecasting design values when fluid velocity is magnified

Finally, magnifications of design values are discussed when the fluid velocity on the inside region of the diffuser is magnified. It means that the correlation between fluid velocity and design values is clarified, and it is expected that the changing scheme of design values is clarified to obtain a higher magnification of fluid velocity.

First, fluid velocity in input data is magnified. The magnified fluid field data is shown in Fig. 9.

As shown in Fig. 9(b), the fluid velocity is magnified in the central area of the fluid field. Inputting the magnified fluid field data to a deep neural network, magnifications (changes) of design values are obtained. The fluid field data with 13 kinds of design values are used. The data is sampled on the same frame. The design values with non-magnified fluid velocity are called h_0, D'_0, and L_0, respectively. The forecasted design values h, D', and L are investigated to clarify the correlation between fluid velocity and design values.

Figure 10 shows the relation between the magnification of fluid velocity v/v_0 and the magnification of design values h/h_0, D'/D'_0, and L/L_0. The horizontal axis shows the magnification of fluid velocity v/v_0 and is on a logarithmic scale. The vertical axis shows the magnification of design values; flange length h/h_0, outlet diameter D'/D'_0, and full-length L/L_0. The solid line shows the average magnification of h/h_0, D'/D'_0, and L/L_0 in 13 kinds of design values. The colored area shows the sample standard deviation of h/h_0, D'/D'_0, and L/L_0.

First, there is a correlation between lengthening flange length h and increase fluid velocity v, as shown in Fig. 10(a). On the average value, flange length h increases by about 1.15 times. Considering the sample standard deviation, the increase of flange length h is between 0.95 and 1.35 times. It indicates an approximate 35% of increase of flange length h at the maximum. Some values indicate a decrease of h. However, since the rate of decrease is low and the amount of data is fewer than the others, it is adequate to express that the flange length h increases. Moreover, the flange length h decreases on the design value No.3 and No.4 in 13 kinds of designs. Then, there is a correlation between slightly lengthening outlet diameter D' and increase fluid velocity v, as shown in Fig. 10(b). On the average value, outlet diameter D' increases by 1.03 times, 3% of the increase. Although the sample standard deviation is considered, the increase of outlet diameter D' is between 0.95 and 1.1 times. The rate of magnification is lower than in the other case. Lastly, there is a correlation between shortening full-length L and increase fluid velocity v, as shown in Fig. 10(c). On the average value, full-length L decreases by 0.91 times. Considering the sample standard deviation, the increase of full-length L is between 0.77 and 1.06 times. It indicates an approximate 23% of decrease of full-length L at the maximum. Some values indicate an increase of L. However, since the rate of increase is low and the amount of data is fewer than the others, it is adequate to express that the full-length L decreases. Moreover, the full-length L increases on the design value No.9 and No.10 in 13 kinds of designs.

In conclusion, there is a trend of correlation between "increase of flange length", "slight increase of outlet diameter", "decrease of the whole length", and "increase of fluid velocity". Although there are some standard deviations in 13 kinds of designs, this trend of correlation will contribute to the decision of design value of tidal/ocean power generators utilizing FFD.

Fig. 10 shows the limitation of the model. Variances of predicted design value increases by getting as far away from the true value(experimental value). However, the limitation of accuracy can be extended if the model learns with experimental data with new condition. Additionally, we aim to measure the fluid field in 3D experimental setting as Fig. 11. This 3D

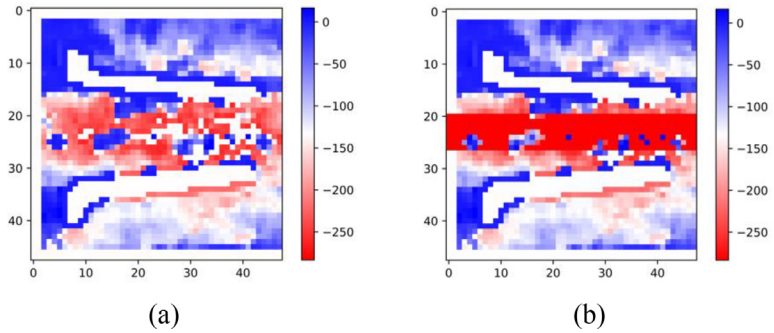

Fig. 9. (a)Original fluid field data and (b)magnified fluid field data. On (b), the fluid velocity is magnified in the central area by ten times.

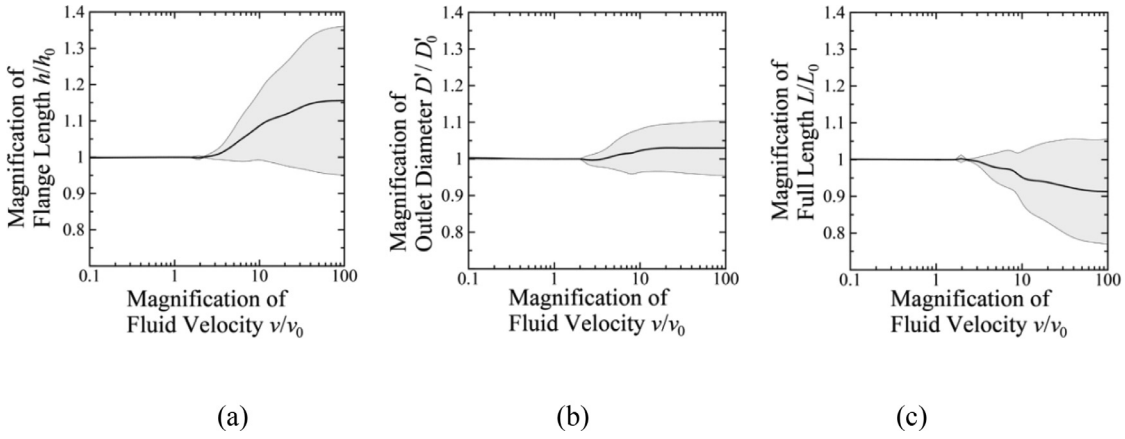

Fig. 10. Relation between the magnification of fluid velocity v/v_0 and the magnification of design values; (a)flange length h/h_0, (b)outlet diameter D'/D'_0, and (c)full length L/L_0. Horizontal axis shows the magnification of fluid velocity v/v_0, and is on logarithmic scale. Vertical axis shows the magnification of design values; flange length h/h_0, outlet diameter D'/D'_0, and full length L/L_0.

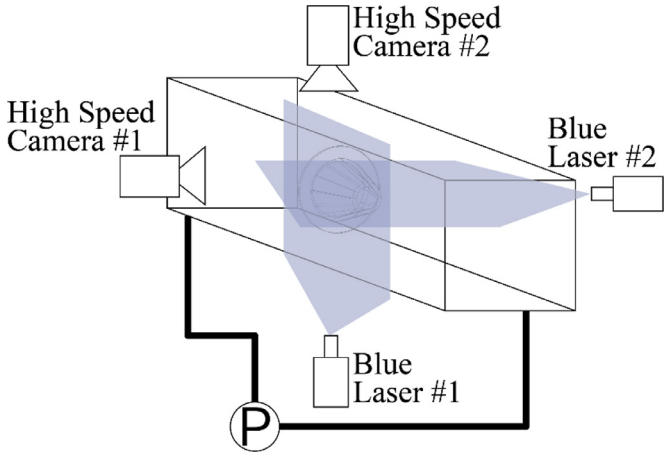

Fig. 11. Experimental setting to measure the fluid field in 3D. Two blue lasers irradiates the particle in the fluid.

fluid field data will contribute to verify the validation of the model.

5. Conclusion

In this paper, the objective was to forecast the design value of tidal/ocean power generators with Flaring Flanged Diffuser (FFD). We were especially interested in the dimensions of the diffuser shape that relate to effective factor for increasing flow velocity.

Fluid field data around FFD is obtained by experimentation. The fluid field data is measured by particle image velocimetry (PIV).

Forecasting design values from a given fluid field is performed by the trained deep neural network. The errors are within almost $\pm 0.1\%$. Thus, it could be expected that design values are forecasted with high accuracy using unknown fluid field data such as interpolation of experimental data. Now, we can decide design values based on the stream regime to efficiently extract tidal/ocean energy by each power generator utilizing FFD in the strait with various streams.

We also investigated the correlation between fluid velocity and design values. There is a trend of correlation between "increase of flange length", "slight increase of outlet diameter", "decrease of whole length", and "increase of fluid velocity". This trend of correlation will contribute to the decision of the design value of tidal/ocean power generators utilizing FFD.

As a future work, the proposed method will be applied to the developments of ocean power generators in various stream regimes.

Declaration of Competing Interest

The authors declare that they have no known competing financial interests or personal relationships that could have appeared to influence the work reported in this paper.

CRediT authorship contribution statement

Ryo Fujiwara: Conceptualization, Methodology, Formal analysis, Data curation, Writing – original draft, Visualization. **Ryoma Fukuhara:** Software, Investigation. **Tsubasa Ebiko:** Validation, Resources. **Makoto Miyatake:** Writing – review & editing, Supervision, Project administration, Funding acquisition.

Acknowledgement

The authors would like to thank Mr. Robert Anthony Olexa of the Department of General Humanities, National Institute of Technology, Hakodate College, for his helpful advice on perspicuous English writing. This work was supported by JSPS KAKENHI Grant Nos. 18H01537 and 21K14081. This work was also supported by Leave a Nest kosen grant Focus Systems award.

References

Abboud, A. W., Fenton, K. R., Lehmer, J. P., Fehringer, B. A., Gentle, J. P., McJunkin, T. R., et al. (2019). Coupling computational fluid dynamics with the high resolution rapid refresh model for forecasting dynamic line ratings. *Electric Power Systems Research, 170*, 326–337. https://doi.org/10.1016/j.epsr.2019.01.035.

Aly, H. H. (2020). A proposed intelligent short-term load forecasting hybrid models of ANN, WNN and KF based on clustering techniques for smart grid. *Electric Power Systems Research, 182*, Article 106191. https://doi.org/10.1016/j.epsr.2019.106191.

Aly, H. H. (2020). Intelligent optimized deep learning hybrid models of Neuro wavelet, Fourier series and recurrent Kalman filter for tidal currents constitutions forecasting. *Ocean Engineering, 218*, Article 108254. https://doi.org/10.1016/j.oceaneng.2020.108254.

Amundarain, M., Alberdi, M., Garrido, A., Garrido, I., & de la Sen, M. (2012). Neural control for wave power plant during voltage dips. *Electric power systems research, 92*, 96–105. https://doi.org/10.1016/j.epsr.2012.06.007.

Atef, S., & Eltawil, A. B. (2020). Assessment of stacked unidirectional and bidirectional long short-term memory networks for electricity load forecasting. *Electric Power Systems Research, 187*, Article 106489. https://doi.org/10.1016/j.epsr.2020.106489.

Bastos, B. Q., Oliveira, F. L. C., & Milidiú, R. L. (2021). Componentnet: Processing U-and V-components for spatio-Temporal wind speed forecasting. *Electric Power Systems Research, 192*, Article 106922. https://doi.org/10.1016/j.epsr.2020.106922.

Bento, P. M. R., Pombo, J. A. N., Mendes, R. P. G., Calado, M. R. A., & Mariano, S. J. P. S. (2021). Ocean wave energy forecasting using optimised deep learning neural networks. *Ocean Engineering, 219*, Article 108372. https://doi.org/10.1016/j.oceaneng.2020.108372.

Bessani, M., Massignan, J. A., Santos, T. M., London, J. B., & Maciel, C. D. (2020). Multiple households very short-term load forecasting using bayesian networks. *Electric Power Systems Research, 189*, Article 106733. https://doi.org/10.1016/j.epsr.2020.106733.

Chen, H., Wang, S., Wang, S., & Li, Y. (2019). Day-ahead aggregated load forecasting based on two-terminal sparse coding and deep neural network fusion. *Electric Power Systems Research, 177*, Article 105987. https://doi.org/10.1016/j.epsr.2019.105987.

Chollet, F. (2017). *Deep learning with python*. Manning Publications.

Gan, Z., Li, C., Zhou, J., & Tang, G. (2021). Temporal convolutional networks interval prediction model for wind speed forecasting. *Electric Power Systems Research, 191*, Article 106865. https://doi.org/10.1016/j.epsr.2020.106865.

Ghefiri, K., Bouallègue, S., Garrido, I., Garrido, A. J., & Haggège, J. (2018). Multi-layer artificial neural networks based MPPT-pitch angle control of a tidal stream generator. *Sensors, 18*(5), 1317. https://doi.org/10.3390/s18051317.

Han, J., Jung, J., & Hwang, J. H. (2021). Optimal configuration of a tidal current turbine farm in a shallow channel. *Ocean Engineering, 220*, Article 108395. https://doi.org/10.1016/j.oceaneng.2020.108395.

Heras-Saizarbitoria, I., Zamanillo, I., & Laskurain, I. (2013). Social acceptance of ocean wave energy: A case study of an OWC shoreline plant. *Renewable and Sustainable Energy Reviews, 27*, 515–524. https://doi.org/10.1016/j.rser.2013.07.032.

Jónsdóttir, G. M., & Milano, F. (2020). Stochastic modeling of tidal generation for transient stability analysis: A case study based on the all-island Irish transmission system. *Electric Power Systems Research, 189*, Article 106673. https://doi.org/10.1016/j.epsr.2020.106673.

Khwaja, A. S., Anpalagan, A., Naeem, M., & Venkatesh, B. (2020). Joint bagged-boosted artificial neural networks: Using ensemble machine learning to improve short-term electricity load forecasting. *Electric Power Systems Research, 179*, Article 106080. https://doi.org/10.1016/j.epsr.2019.106080.

Kingma, D.P., .& Ba, J.L. (2014). Adam: A method for stochastic optimization. arXiv preprint arXiv:1412.6980. https://arxiv.org/pdf/1412.6980.pdf

Liu, M., Li, W., Billinton, R., Wang, C., & Yu, J. (2015). Modeling tidal current speed using a Wakeby distribution. *Electric Power Systems Research, 127*, 240–248. https://doi.org/10.1016/j.epsr.2015.06.014.

Liu, X., Zhou, J., & Qian, H. (2021). Short-term wind power forecasting by stacked recurrent neural networks with parametric sine activation function. *Electric Power Systems Research, 192*, Article 107011. https://doi.org/10.1016/j.epsr.2020.107011.

Lust, E. E., Bailin, B. H., & Flack, K. A. (2021). Performance characteristics of a cross-flow hydrokinetic turbine in current only and current and wave conditions. *Ocean Engineering, 219*, Article 108362. https://doi.org/10.1016/j.oceaneng.2020.108362.

Marei, M. I., Mokhtar, M., & El-Sattar, A. A. (2015). MPPT strategy based on speed control for AWS-based wave energy conversion system. *Renewable Energy, 83*, 305–317. https://doi.org/10.1016/j.renene.2015.04.039.

Mehmood, N., Liang, Z., & Khan, J. (2012). Diffuser augmented horizontal axis tidal current turbines. *Research Journal of Applied Sciences, Engineering and Technology,. 4*(18), 3522–3532.

Memarzadeh, G., & Keynia, F. (2021). Short-term electricity load and price forecasting by a new optimal LSTM-NN based prediction algorithm. *Electric Power Systems Research, 192*, Article 106995. https://doi.org/10.1016/j.epsr.2020.106995.

M'zoughi, F., Garrido, I., Garrido, A. J., & De La Sen, M. (2020). Rotational speed control using ANN-Based MPPT for OWC based on surface elevation measurements. *Applied Sciences, 10*(24), 8975. https://doi.org/10.3390/app10248975.

M'zoughi, F., Garrido, I., Garrido, A. J., La Sen, D., & De La, M. (2020). ANN-based airflow control for an oscillating water column using surface elevation measurements. *Sensors, 20*(5), 1352. https://doi.org/10.3390/s20051352.

New Energy and Industrial Technology Development Organization, NEDO to conduct World's first 100 kW class demonstration test of ocean current power generation (accessed 29 Jun. 2021) https://www.nedo.go.jp/english/news/AA5en_100269.html.

Riddervold, H. O., Riemer-Sørensen, S., Szederjesi, P., & Korpås, M. (2020). A supervised learning approach for optimal selection of bidding strategies in reservoir hydro. *Electric Power Systems Research, 187*, Article 106496. https://doi.org/10.1016/j.epsr.2020.106496.

Ryu, A., Ishii, H., & Hayashi, Y. (2021). Battery smoothing control for photovoltaic system using short-term forecast with total sky images. *Electric Power Systems Research, 190*, Article 106645. https://doi.org/10.1016/j.epsr.2020.106645.

Sideratos, G., Ikonomopoulos, A., & Hatziargyriou, N. D. (2020). A novel fuzzy-based ensemble model for load forecasting using hybrid deep neural networks. *Electric Power Systems Research, 178*, Article 106025. https://doi.org/10.1016/j.epsr.2019.106025.

Suchithra, R., Ezhilsabareesh, K., & Samad, A. (2019). Optimization-based higher-order sliding mode controller for efficiency improvement of a wave energy converter. *Energy, 187*, Article 116111. https://doi.org/10.1016/j.energy.2019.116111.

Toubeau, J. F., Dapoz, P. D., Bottieau, J., Wautier, A., De Grève, Z., & Vallée, F. (2021). Recalibration of recurrent neural networks for short-term wind power forecasting. *Electric Power Systems Research, 190*, Article 106639. https://doi.org/10.1016/j.epsr.2020.106639.

Wen, L., Zhou, K., & Yang, S. (2020). Load demand forecasting of residential buildings using a deep learning model. *Electric Power Systems Research, 179*, Article 106073. https://doi.org/10.1016/j.epsr.2019.106073.

Wen, Z., Xie, L., Fan, Q., & Feng, H. (2020). Long term electric load forecasting based on TS-type recurrent fuzzy neural network model. *Electric Power Systems Research, 179*, Article 106106. https://doi.org/10.1016/j.epsr.2019.106106.

Wilberforce, T., El Hassan, Z., Durrant, A., Thompson, J., Soudan, B., & Olabi, A. G. (2019). Overview of ocean power technology. *Energy, 175*, 165–181. https://doi.org/10.1016/j.energy.2019.03.068.

Xia, M., Wang, K., Zhang, X., & Xu, Y. (2019). Non-intrusive load disaggregation based on deep dilated residual network. *Electric Power Systems Research, 170*, 277–285. https://doi.org/10.1016/j.epsr.2019.01.034.

Zheng, C., Wang, S., Liu, Y., & Liu, C. (2019). A novel RNN based load modeling method with measurement data inactive distribution system. *Electric Power Systems Research, 166*, 112–124. https://doi.org/10.1016/j.epsr.2018.09.006.

Zhu, K., Geng, J., & Wang, K. (2021). A hybrid prediction model based on pattern sequence-based matching method and extreme gradient boosting for holiday load forecasting. *Electric Power Systems Research, 190*, Article 106841. https://doi.org/10.1016/j.epsr.2020.106841.